Glycosylation analysis of immune-related molecules

Borosak, I.

[1] *Center for Proteomics and Metabolomics, Leiden University Medical Center, Leiden, The Netherlands*

[2] *Glycoscience Research Laboratory, Genos Ltd., Zagreb, Croatia*

[3] *Department of Experimental Immunohematology, Sanquin Research, and Landsteiner Laboratory, Academic Medical Center, University of Amsterdam, Amsterdam, The Netherlands*

[*] *Authors share co-first autorship*

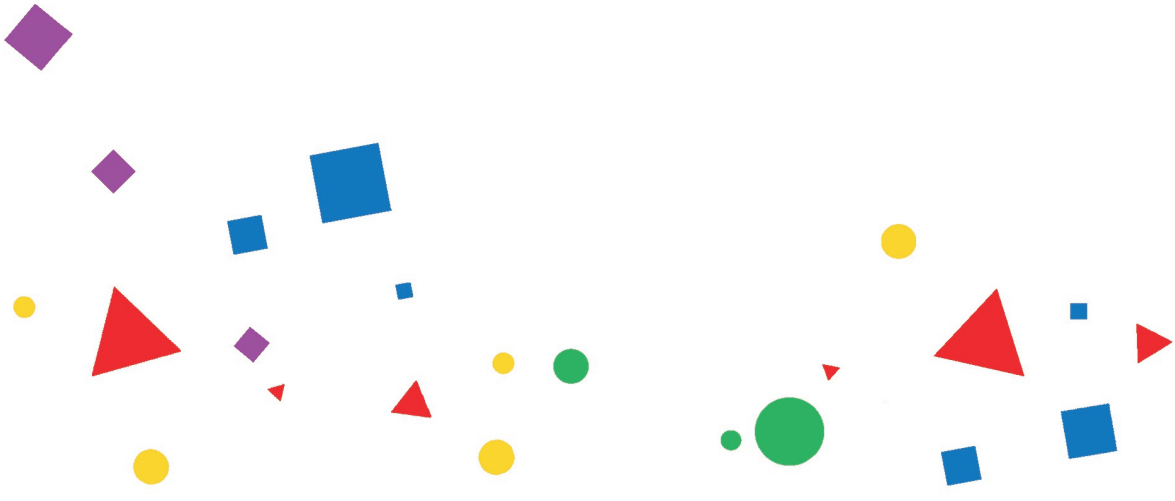

Chapter 4

Site-specific glycosylation mapping of Fc gamma receptor IIIb from neutrophils of individual healthy donors

Iwona Wojcik[1,2*], Thomas Sénard[1*], Erik L de Graaf[3], George MC Janssen[1], Arnoud H de Ru[1], Yassene Mohammed[1], Peter A van Veelen[1], Gestur Vidarsson[3], Manfred Wuhrer[1] and David Falck[1]

Reprinted and adapted with permission from

Anal Chem. 2020 Oct 6;92(19):13172-13181. doi: 10.1021/acs.analchem.0c02342. Epub 2020 Sep 22. PMID: 32886488; PMCID: PMC7547861.

4.1 ABSTRACT

Fc gamma receptors (FcγRs) translate antigen-recognition by immunoglobulin G (IgG) into various immune responses. A better understanding of this key element of immunity promises novel insights into mechanisms of (auto-/allo-)immune diseases and more rationally designed antibody-based drugs. Glycosylation on both IgG and FcγR impacts their interaction dramatically. Regarding FcγR glycosylation profiling, major analytical challenges are associated with the presence of multiple glycosylation sites in close proximity and the large structural heterogeneity. In order to address these challenges, we developed a straightforward and comprehensive analytical methodology to map FcγRIIIb glycosylation from primary human cells. After neutrophil isolation and immunoprecipitation, glycopeptides containing a single site each were generated by a dual-protease in-gel digestion. The complex mixture was resolved by liquid chromatography - tandem mass spectrometry (LC-MS/MS) providing information on the level of individual donors. In contrast to recently published alternatives for FcγRIIIb, we assessed its site-specific glycosylation in a single LC-MS/MS run and simultaneously determined the donor allotype. Studying FcγRIIIb derived from healthy donor neutrophils, we observed profound differences as compared to the soluble variant and the homologous FcγRIIIa on natural killer cells. This method will allow assessment of FcγRIII glycosylation differences between individuals, cell types, subcellular locations and pathophysiological conditions.

GRAPHICAL ABSTRACT

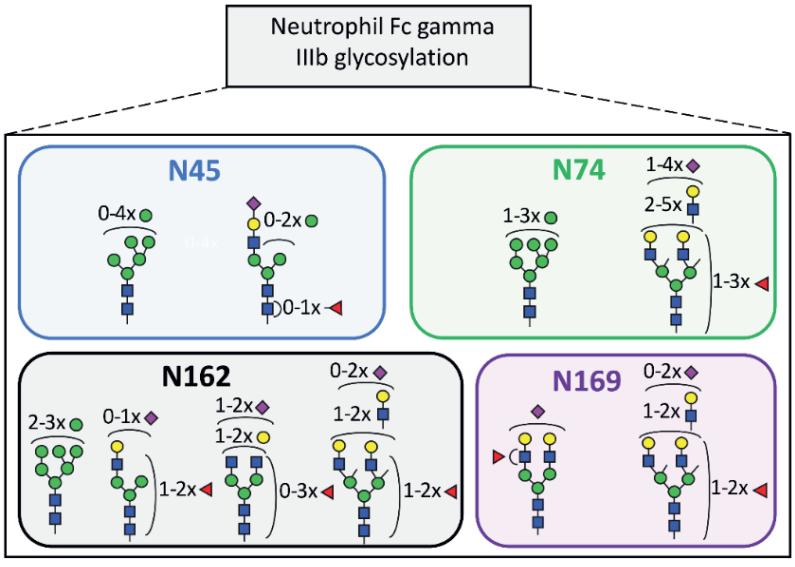

4.2 INTRODUCTION

Binding of immunoglobulin G (IgG) to Fc gamma receptors (FcγRs) initiates and regulates important immune responses.(1, 2) Therefore, FcγRs have a key role in homeostasis and in many pathological conditions.(3, 4) This is widely exploited for therapeutic purposes, for example with monoclonal antibodies or polyclonal intravenous IgG.(5-7) The key interaction between IgG and FcγRs is heavily regulated by the proteoform distribution of either binding partner, e.g. through post-translational modifications. The impact of IgG proteoforms has been extensively studied in the last decades.(8, 9) Subclass, allotype and glycosylation, especially (a)fucosylation, of IgG impact FcγR binding.(10-12) FcγR-mediated IgG effector functions are partially regulated by varying FcγR expression on different immune cells.(13) For example, FcγRIIIb or CD16b is exclusively expressed as a monomeric protein mainly on granulocytes, while the homologous FcγRIIIa or CD16a is expressed on NK cells, monocytes, macrophages and dendritic cells. Unlike all other transmembrane FcγRs, the human FcγRIIIb is GPI-anchored and lacks a transmembrane and cytoplasmic signalling domain. FcγRIIIb is an 233 amino acid protein which consists of N-terminal signal peptide (18 amino acids) cleaved during protein processing and two domains in the extracellular region.(14) Those domains share 97% sequence homology with FcγRIIIa.(15) Despite the homology, FcγRIIIa binds IgG stronger than FcγRIIIb due to a single amino acid difference, G_{129} versus D_{129}.(16) FcγRIIIb seems to affect signalling of other Fc-receptors through accumulation in lipid rafts which are enriched in kinases (Src) and required for ITAM-phosphorylation and signalling.(17) Given the relatively high expression levels of FcγRIIIb on neutrophils with 120,000 to 300,000 copies per cell,(18) and the dominance of neutrophils amongst white blood cells, FcγRIIIb can be considered the most abundant FcγR in circulation. Known functions include activation of neutrophil degranulation, cell adhesion, calcium mobilization and neutrophil tethering to soluble immune complexes.(19-21)

Despite recent advances, the role of FcγR proteoforms is only poorly understood.(14) Allotypes lead to differentially active proteoforms. There are three known allotypes of FcγRIIIb, neutrophil antigen 1 (NA1) and 2 (NA2), and SH (SH being uncommon). They vary in their affinity for IgG and capacity to induce phagocytosis of IgG-opsonized targets.(22) The two major FcγRIIIb allotypes, NA1 and NA2 differ in four amino acids , resulting in four and six potential *N*-glycosylation sites for NA1 (N_{38}, N_{74}, N_{162}, N_{169}) and NA2 (N_{38}, N_{45}, N_{64}, N_{74}, N_{162}, N_{169}), respectively.(23) Five of the potential N-glycosylation sites are conserved between FcγRIIIa and FcγRIIIb, namely N38, N45, N74, N162 and N169. The vast majority of glycan data on FcγRIII derives from the endogenous FcγRIIIa from NK cells(24) and monocytes,(25) as well as recombinant protein expressed in human embryonic kidney (HEK), Chinese hamster ovary (CHO) cells,(26) Baby Hamster Kidney Cells (BHK)(27) and murine cell line NS0.(28) Both variants, endogenous as well as a recombinant FcγRIIIa/b are modified by *N*-glycans, but only for recombinant FcγRIIIa a single *O*-glycan modification has been detected.(26) FcγR glycosylation strongly impacts the interaction with IgG. Some

receptor glycans have direct glycan-glycan and glycan-protein interactions with bound IgG.(29, 30) Deglycosylation of site N_{162} (unique to FcγRIIIa and FcγRIIIb), strongly elevates affinity of FcγRIIIa to IgG, but also alleviates sensitivity to IgG-core-fucosylation.(31, 32) Furthermore, differences in FcγRIIIb glycosylation in different cell models, have been shown to impact IgG binding.(33, 34) The available studies underline the importance of FcγR glycosylation, but can so far only sketch a very rough picture of its functional impact.

A prominent reason for this lack of functional understanding is the limited available data on FcγR glycosylation of primary human cells.(14) While the great heterogeneity of proteoforms, especially in FcγRIIIb, was already apparent in early studies,(18) glycomics studies on primary human cells only became possible in recent years.(35) However, owing to the great complexity and differential functional impact of glycosylation sites, only site-specific glycoproteomics studies can characterize FcγR glycosylation to the necessary extent. Recent studies on healthy volunteers revealed FcγRIIIa glycosylation of NK cells(24) and monocytes(25) and FcγRIIIb glycosylation of neutrophils(36). Therein, cells were purified by negative selection with magnetic beads, followed by immunoprecipitation of FcγR. Additionally, the soluble FcγRIIIb,(37) which originates from shedding from neutrophils upon their activation, has been studied in plasma. The purified receptor from all sources was analysed by bottom-up glycoprotein analysis / glycoproteomics following protease cleavage with chymotrypsin and/or endoproteinase Glu-C (GluC).(26) Targeted analysis of FcγRIIIb using immunoprecipitation (IP) offers important advantages, because it increases the depth of analysis, and hence the number of identified and quantified glycoforms. Untargeted glycoprofiling strategies possess the advantage that they provide a glimpse on the glycosylation of many proteins. While they may overcome potential proteoform-biases in antibody-specificity for IP, the increased sample complexity and resulting co-elution of (glyco-)peptides in such approaches introduce significant biases due to ion-suppression and undersampling.(38, 39)

While ground-breaking, the two previous studies on site-specific glycosylation of FcγRIIIb had some limitations.(36, 37) They relied on two independent proteolytic cleavages, thus necessitating multiple liquid chromatography – mass spectrometry (LC–MS) runs to cover the whole receptor. Yagi *et al.* focused on soluble FcγRIIIb whose function is largely unknown.(37) They used pooled blood from multiple donors, losing inter-donor variability. Washburn *et al.* only analysed three of the six potential *N*-glycosylation sites, but accumulated strong data on inter-donor variability of 50 donors.(36) Nonetheless, we still know too little about the functional and clinical impact of FcγR glycosylation to prefer a method focussing only on certain glycosylation sites. Other existing strategies covering all sites of FcγRIIIb or FcγRIIIa are quite complicated to apply to clinical investigations where eventually large numbers of samples need to be detected in a robust way.(24, 37)

Here, we present a method for the site-specific analysis of all glycosylation sites of FcγRIIIb in a single LC-MS/MS experiment. With it, we identified and relatively quantified neutrophil-derived FcγRIIIb glycosylation individually for multiple donors. Additionally, our approach allowed a qualitative overview of site occupancy and the determination of donor allotypes. This was enabled by avoiding glycopeptide enrichment which also promises more robustness. Additionally, interferences from endogenous IgG and from leaking capturing antibody are avoided by a simple non-reducing SDS-PAGE step. Additionally, our method is generic for FcγRIIIa and FcγRIIIb, making it potentially applicable to a wide range of leukocytes. Moving towards clinical investigations of FcγR glycosylation will be essential for a complete understanding of the (patho-)physiological role of IgG-FcγR interactions. Our methodology presents a uniquely suited starting point, as it is unprecedented in its ability to simultaneously cover individual donor, subclass, allotype, cell and site differences of FcγRIII glycosylation comprehensively.

4.3 EXERIMENTAL SECTION

4.3.1 Buffers and reagents

Trizma hydrochloride, Tris(hydroxymethyl)aminomethane, Protease Inhibitor Cocktail (Set V, EDTA-Free), phenylmethylsulfonyl fluoride (PMSF), ethylenediaminetetraacetic acid (EDTA), glycerol were obtained from Sigma-Aldrich (Steinheim, Germany). Di-sodium hydrogen phosphate dihydrate (Na2HPO4·2 H2O), potassium dihydrogen phosphate (KH2PO4), and NaCl were obtained from Merck (Darmstadt, Germany). CARIN lysis buffer (pH 8.0) was prepared in-house with 20 mM Tris-HCl, 137 mM NaCl, 10 mM EDTA, 0.1 M NaF, 1% NP-40 and 10% glycerol. Protease Inhibitor Cocktail and PMSF were added to prevent unwanted proteolysis. Phosphate-buffered saline (PBS, 0.035 M, pH 7.6) was prepared in-house with 5.7 g/L of Na2HPO4, 2 H2O, 0.5 g/L of KH2PO4, and 8.5 g/L of NaCl. Coomassie staining was prepared in-house according to Candiano et al.(40) using Coomassie Blue G-250 (Sigma-Aldrich). SDS-PAGE reagents were of the NuPAGE™ series (ThermoFisher Scientific) and included: LDS Sample Buffer (4x) (non-reducing loading buffer), a PageRuler Prestained Protein Ladder (protein standard), 4-12% Bis-Tris gel and a 4 Morpholinepropanesulfonic acid (MOPS) SDS running buffer.

4.3.2 Materials

GluC (Staphyloccoccus aureus Protease V8) and chymotrypsin were obtained from (Worthington Biochemical Corp., Lakewood, USA). The ultrapure deionized water (MQ) was generated using a Q-Gard 2 system (Millipore, Amsterdam, Netherlands). MS grade acetonitrile (ACN) was acquired from Biosolve B.V. (Valkenswaard, The Netherlands). Iodoacetamide (IAA), dithiothreitol (DTT), ethylenediaminetetraacetic acid (EDTA), analytical grade formic acid (FA) and LC-MS grade water were obtained from Sigma-Aldrich (Steinheim, Germany). More information on buffers and reagents can be found in the

Supplementary Information. FcγRIIIs were immunoprecipitated from the neutrophil cell lysate using a mouse anti-CD16 monoclonal IgG2a antibody (Ref M9087, Clone CLB-FcR gran/1, 5D2, Sanquin, Amsterdam, The Netherlands). Prior to usage, antibodies were labelled with biotin.

4.3.3 Antibody biotinylation

At first, antibodies were buffer exchanged from Tris buffer to PBS buffer using the Zeba spin protocol (ThermoFisher Scientific, Rockford, IL, USA), as amine-containing buffers may interfere with biotinylation. Subsequently, the Z-link™ Sulfo-NHS-Biotinylation protocol (ThermoFisher Scientific) was followed. The level of biotin incorporation was measured with a HABA Assay (ThermoFisher Scientific).

4.3.4 Neutrophil cell isolation and FcγRIIIb purification

Neutrophils were isolated from whole blood of three healthy volunteers as described previously.(41) Briefly, the blood was collected from healthy donors into tubes coated with spray dried EDTA for anticoagulation (VACUETTE TUBE 9ml K3E K3EDTA, Greiner Bio-One, Amsterdam, Netherlands). Mononuclear leukocytes and platelets were removed by centrifugation (2,000 rpm, 18 min, 25°C) using a Ficoll gradient with a specific density of 1.077 g/mL (Ficoll-Paque PLUS, GE Healthcare, Freiburg, Germany). Erythrocytes were subsequently lysed with isotonic NH_4Cl solution at 4°C. With this standard method, a high degree of depletion of other cell types is obtained and neutrophils are isolated with a typical purity of over 95%. The isolated neutrophils were washed two times with 1 mL of cold PBS. The cells were counted on a CASY automated cell counter (Thermo Fisher Scientific, Rockford, IL, USA) followed by centrifugation (1,200 rpm, 4 minutes, 4°C). The neutrophils were resuspended in CARIN Buffer at a final concentration of 50 x 10^6 cells/mL (**Table S1**). The cells were then incubated on ice for 5-10 min. Lastly, cell lysates were sonicated for 30 seconds at 20 kHz. The cell lysate was centrifuged at 13000 x *g* for 15 min at 4°C. The cellular debris pellet was discarded. The total protein content of the supernatant was measured with a NanoDrop™ 2000 spectrophotometer (Thermo Fisher Scientific, Rockford, IL, USA). For FcγRIII identification and purification, respectively, an amount of ∼3 or ∼16 million primary human neutrophils from healthy donors was used for immunoprecipitation (**Table S1**). 100 µg or 500 µg of neutrophil proteins were incubated, while rotating, with 5 µg or 25 µg of biotinylated antibodies in the total volume of 1 mL CARIN lysis buffer overnight at 4°C. A rough estimate of the antibody: FcγRIII ratio was 2,500:1. 10 µL of High Capacity Streptavidin Agarose Resin beads (Thermo) were washed twice in 1 mL CARIN buffer and incubated with the pre-formed FcγRIII-anti-CD16 immune complexes for 1 hour at 4°C and rotating. The beads were centrifuged for 2 min at 2500 x *g*, removing supernatant, and washed four times with 1 mL CARIN buffer. Finally, FcγRIII was eluted from the beads with

two times 150 µL of 200 mM FA. The eluates were then dried by vacuum centrifugation at 60°C for 2 hours.

4.3.5 SDS-PAGE

The immunoprecipitation of FcγRIIIb from 100 µg of total neutrophil proteins was evaluated by sodium dodecyl-sulfate-polyacrylamide gel electrophoresis (SDS-PAGE). The dried samples were resuspended in 20 µL of non-reducing loading buffer, incubated at 95°C for 5 min and applied to a 4-12% Bis-Tris gel. The migration was performed at 200 V constant voltage for 50 min in 4-Morpholinepropanesulfonic acid (MOPS) SDS running buffer. Gels were stained using Coomassie blue. The presence of CD16 was confirmed by western blotting, using an anti-CD16 mouse monoclonal IgG1 conjugated to horseradish peroxidase (DJ130c, sc-20052 HRP, Lot #D2617, Santa Cruz Biotech; see also Supplementary Information).

4.3.6 In-gel proteolytic digest and LC-MS glycopeptide analysis

For the in-gel LC-MS workflow, 500 µg of total neutrophil proteins were used for immunoprecipitation. The subsequent SDS-PAGE was performed at 200 V constant voltage for only 15 min. The obtained gels were silver stained (SilverQuest™ Staining Kit, Invitrogen) and the protein of interest was cut out from the gel. Excised bands were subjected to in-gel digestion with endoproteinase GluC and chymotrypsin which was performed on a Proteineer DP digestion robot (Bruker, Bremen, Germany).(26, 42, 43) Reduction with 10 mM DTT was followed by alkylation with 50 mM IAA(44) and 3 wash and shrink cycles with 25 mM ammonium bicarbonate (pH 8.4) and neat acetonitrile, respectively. The shrunken gel bands were soaked for 45 min at 10°C in 25 mM ammonium bicarbonate, containing both proteases at a concentration of 12.8 ng/ml each. Excess protease solution was removed, followed by overnight digestion at 37°C. Peptides were extracted with 100 µl H_2O/acetonitrile/ formic acid (50/50/1), lyophilized and dissolved in solvent A (3% ACN/95% water containing 0.1% FA (v/v)) prior to injection. The liquid chromatography-tandem mass spectrometry (LC-MS/MS) analysis was performed on a nanoLC-MS system composed of an Easy nLC 1000 gradient HPLC system (Thermo, Bremen, Germany) and a LUMOS mass spectrometer (Thermo). Prior to sample injection, the peptides and glycopeptides extracted from the bands were lyophilized and dissolved in solvent A (water containing 0.1% FA (v/v)). The samples were then loaded onto an in-house packed C18 precolumn (100 µm × 15 mm; Reprosil-Pur C18-AQ 3 µm, Dr. Maisch, Ammerbuch, Germany) and separated on a homemade analytical nanoLC column (30 cm × 75 µm; Reprosil-Pur C18-AQ 3 µm). The digested (glyco-)peptides were eluted using a linear gradient from 10 to 40% solvent B (80% ACN/20% water containing 0.1% FA (v/v)) over 20 min, followed by a column washing step with solvent B to 100% (at 25 min) and reconditioning with solvent A for 12 min. The nanoLC column was drawn to a tip of ∼5 µm and acted as the electrospray needle of the MS source. The Orbitrap Fusion LUMOS mass spectrometer was operated in data-dependent MS/MS

(top-20 mode) with the collision energy set at 32% normalized collision energy (NCE) and recording the MS/MS spectrum in the Orbitrap. The MS^1 full scan spectra were acquired within a mass range of *m/z* of 400–1500 and MS/MS was set to auto (i.e. depending on the m/z of the selected precursor ion). The resolution setting for MS^1 scans was 12×10^4 and an AGC target value of 4×10^4 for an accumulation time of a maximum 50 ms. Dynamic exclusion duration was 10 s with a single repeat count, and charge states in the range 1–5 were included for MS/MS. The resolution of MS/MS scans was 3×10^4 with an AGC target of 5×10^4 with a maximum fill time of 60 ms. MS/MS spectra were generated from precursors isolated with the quadrupole with an isolation width of 1.2 Da. During acquisition, a product ion trigger was set on the HexNAc oxonium ion at m/z 204.087. Upon the detection of the oxonium ion, three additional data-dependent MS/MS scans of the same precursor were executed in the ion-routing multipole with higher-energy collisional dissociation (HCD) collision energies of 32%, 37%, and 42% NCE, respectively, at an AGC target of 5×10^5 with a maximum fill time of 200 ms. In addition, the acquisition of collision-induced dissociation (CID) spectra in the linear ion trap was performed for the precursor and recorded at 35% NCE. The presented results on protein identification, coverage and purity are from a standard data-dependent HCD run (without exclusive *m/z* 204.087 triggering). For the identification of glycopeptides in these runs, MS/MS spectra containing the specific HexNAc oxonium ion at m/z 204.087 (HexNAc, $[C_8H_{14}NO_5]^+$) were extracted from the raw data and written to a .mgf file using in-house routines. This filtering step also ensured to include only spectra containing the HexNAc oxonium ion with a strong signal (among top 30 peaks).

4.5.7 Identification and quantification of site-specific glycosylation

Initially, LC-MS/MS data were processed with Byonic (Protein Metrics, Cupertino, CA v3.2-38).(45) MS/MS spectra were searched against an extensive human proteome database combined with a pre-defined glycan list (**Table S2**). Glycopeptides identification with Byonic scores below 150 were removed from the analysis. Digestion specificity was set as non-specific (slowest), allowing for both specific and miscleaved peptides. Glycosylation was set as a common modification and other modifications were anticipated upon prevalence: Glycan modification/ + [glycan composition] Da @ NGlycan | common1; carbamidomethyl/ +57.021 Da @C | fixed; oxidation/ +15.995 Da @M | common2; acetyl/ +42.011 Da @Protein *N*-term | rare1. The Byonic search allowed one common modification and one rare modification per peptide. For more parameters refer to **Table S3.** Byonic identifications were manually verified and extended using Xcalibur (Thermo). **Table S4** gives an overview of the identification level of individual glycoforms (Byonic, manual MS/MS, manual MS). Regarding the manual identification, MS^1 sum spectra were generated — around the retention times reported by Byonic — and searched for expected monosaccharide differences. This was done per combination of unique peptide backbone and number of sialic acids, the main two retention time determinants. Some sialic acid variants were

inferred, improving the identification of multisialylated glycan compositions. Annotation of MS^1 spectra was based on precursor mass with a tolerance of ± 0.05 Th. Manual MS/MS interpretation was based on, firstly the clear presence of an *m/z* corresponding to a peptide or peptide+HexNAc fragment ion of a previously identified glycosylated sequence and secondly the presence of a dominating pattern of oxonium ions. During the manual interpretation, differences in (glyco-)peptide sequences between the FcγRIIIb allotypes, NA1 and NA2, were taken into consideration.

For automatic alignment, integration and extraction of LC-MS data, the in-house software LacyTools (Version 1.1.0-alpha) was used as described previously.(46) As an input, the raw data files were converted to mzXML files and a list of identified glycopeptides along with their retention times was created. For the area integration of the sum spectra, the following settings were applied: sum spectrum resolution of 100, extraction mass window of 0.07 Th, extraction time window of 15 s, percentage of the theoretical isotopic pattern of 95%, min charge stage 2, max charge stage 4. This resulted in integrated signal intensities for each glycopeptide per charge stage (from $[M+2H]^{2+}$ to $[M+4H]^{4+}$). After extraction, analytes were curated from the identification list, if the average mass error was outside ±20 ppm and the isotopic pattern deviated more than 20% from the theoretical one. This resulted in the exclusion of signals for all doubly charged glycopeptides and inclusion of signals for triply and some quadruply charged analytes. All included charge stage signals for the same glycopeptide were summed, the absolute intensities were corrected for the fraction of isotopes integrated and used for relative quantification. Total area normalization per glycosylation site was used for relative quantitation. The intensities of the iron adduct ($[M+Fe^{III}]^{3+}$) and ammonia adduct ($[M+2H+NH_4]^{3+}$) signals were significant. Hence, the relative quantification was performed on extracted areas of protonated, iron adduct and ammonia adduct peaks. The *N*-glycosylation site occupancy was determined as the fraction of all glycopeptide signals in the sum of glycopeptide and non-glycosylated peptide signals.

4.4 RESULTS AND DISCUSSION

4.4.1 FcγRIIIb purification and identification

Similar to previous reports,(47) the western blot showed a smear from 50 to 80 kDa, confirming the presence of FcγRIIIb with its abundant and diverse glycosylation pattern (**Figure 1**). A comparison of total cell lysate, flow-through and eluate demonstrates the efficacy of the purification. The non-reducing SDS-PAGE allowed the separation of FcγRIIIb from interferences derived, for example, from the capturing antibody or endogenous IgG (**Figure S1**). This is simple and preferable to an affinity removal of IgG which may lose specific FcγR proteoforms due to high affinity interactions.(24) In the eluate, the FcγRIIIb could not be detected by Coomassie blue staining (LOD ca. 25 ng for well-defined bands). This indicated a recovery value below 4 to 20%, determined by the percentage ratio of the eluted FcγRIIIb (< 25 ng) to the theoretical amount of FcγRIIIb on the neutrophil surface

(160-630 ng). This is consistent with the western blot, where the eluate fraction is significantly lower from the neutrophils signal corresponding to the ¼ of the expected optical density at 100%. Despite the low recovery, the purification scheme resulted in enough material for LC-MS(/MS) analysis after in-gel digestion. Furthermore, MS/MS analysis of the purified protein yielded a sequence coverage of approximately 80% and did not indicate any major interferences in the relevant gel band (**Table S5**). Thus, a strong enrichment of FcγRIIIb from neutrophil lysate was achieved.

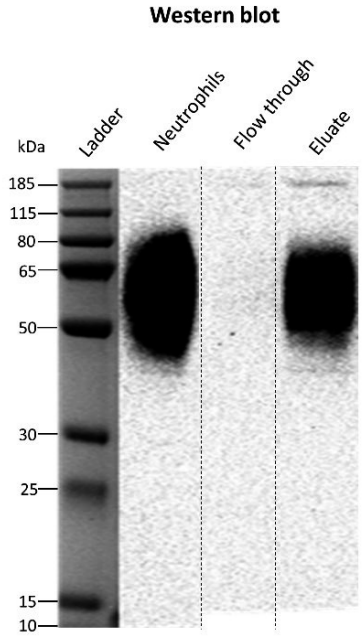

Figure 1. *Western blot of human neutrophil lysate before and after FcγRIII immunoprecipitation. The identity of FcγRIIIb was confirmed with an anti-CD16 antibody. The flow-through lanes show the diluted* unbound *fraction of the immunoprecipitation while the eluate lanes present the purified FcγRIIIb protein. The neutrophil lanes represent ~25 µg of total protein content from the neutrophil cell lysate from donor 2. Apparent differences in the western blot are due to concentration differences. The weaker signal of extremer low and high MW proteoforms is lost at lower concentrations after IP. The cropping area is indicated by striated lines. The complete gel and blot are presented in Figure S1 and Figure S2.*

4.4.2 Coverage and protein identity

Isolated FcγRIIIb was subjected to an in-gel endoproteinase GluC and chymotrypsin treatment prior to the LC-MS(/MS) analysis.(26) This approach was sufficient to generate and identify unique peptides for all six glycosylation motifs. FH**N$_{45}$**ESLISSQASSY (NES), FIDAATV**N$_{64}$**DSGEY (NDS), RCQT**N$_{74}$**LSTLSDPVQLE (NLS), CRGLVGSK**N$_{162}$**VSSE (NVS) and TV**N$_{169}$**ITITQGLAV (NIT) were found in human neutrophils (**Table S6**), while SPED**N$_{38}$**ESQW was only detected in recombinant receptor (**Figure S3 and S4**). An overview of FcγRIIIb

glycopeptides is depicted in **Figure 2**. Our method required only one LC-MS/MS run to obtain full coverage of all glycosylation sites.

FcγRIIIb showed lower electrophoretic mobility for Donor 1, suggesting the less glycosylated NA1 allotype (**Figure S2**). The allotype can be determined by proteomics,(36) which we achieved simultaneously with the glycoprofiling. The assignments were based on the intensity ratios of allele-specific peptides: for example, FHN$_{45}$ENLISSQASSY (NEN), FIDAATVD$_{64}$DSGEY (DDS) for NA1, and FH**N$_{45}$**ESLISSQASSY (NES), FIDAATV**N$_{64}$**DSGEY (NDS) for NA2 (**Table S7**). Indeed, Donor 1 was an NA1/NA2 individual, with a 1:5 ratio of NA2 N$_{45}$ oligomannose glycopeptides (NES/(NES+NEN)). Relative quantitation may be biased by the reduced ionization efficiency of glycopeptides compared to non-glycosylated peptides. However, a similar ratio (1:4) for unoccupied NA2 N$_{64}$ peptide (NDS/(DDS+ NDS)) was observed. Thus, the 1:5/1:4 ratio likely reflects the real expression levels between NA2 and NA1, potentially caused by naturally occurring gene copy number variation of FcγRIIIb.(48) Donors 2 and 3 were NA2 homozygous, since they contained approximately 98% of FH**N$_{45}$**ESLISSQASSY and FIDAATV**N$_{64}$**DSGEY peptides (**Table S7**). The residual 2% was explained by shared peptides sequences between FcγRIIIb NA1 and FcγRIIIa (FHN$_{45}$ENLISSQASSY, FIDAATVD$_{64}$DSGEY and FIDAATVD$_{64}$DSGEYR). We cannot exclude that these signals may be derived from contamination by NK cells, macrophages and/or monocytes. Additionally, deamidation of site N$_{64}$ may contribute to the D$_{64}$ peptide signals, but does not explain the N$_{45}$ signals. Importantly, at these low levels, the impact of FcγRIIIa glycopeptides on FcγRIIIb glycosylation profiling can be neglected. Therefore, co-isolation is preferred as it enables the use of the same sample preparation protocol for FcγRIIIa-dominated cell types.

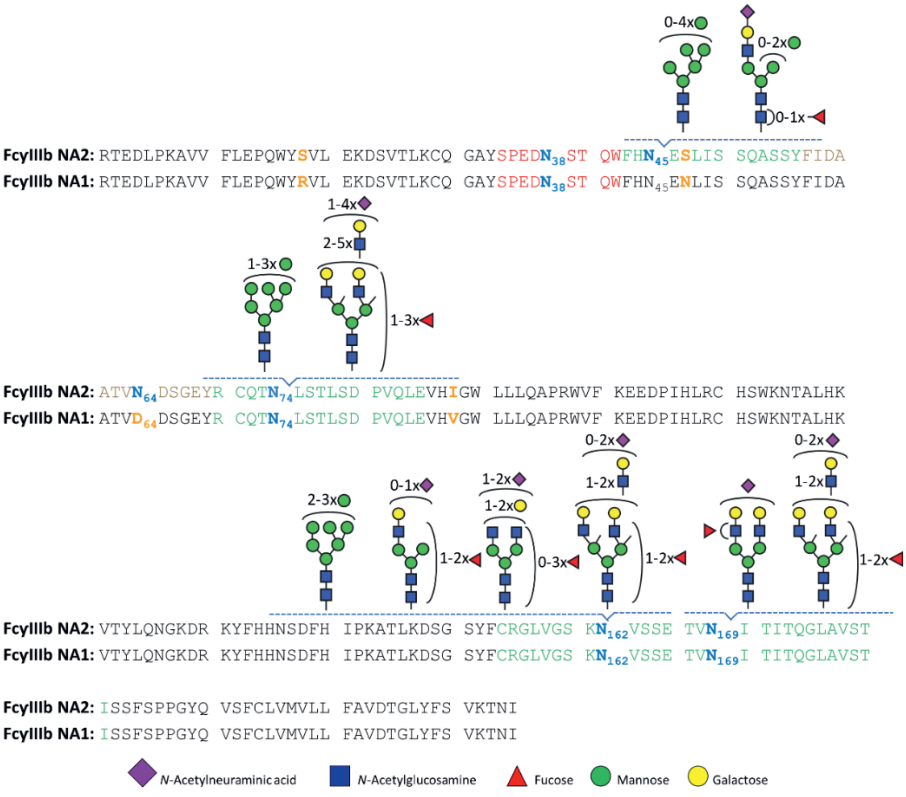

Figure 2. *A schematic representation of site-specific N-glycosylation of endogenous FcγRIIIb NA1 and NA2 from human neutrophils. N-glycosylation sites are noted in bold, blue letters. All determined and occupied glycopeptides are depicted in green with their corresponding set of glycans. A peptide with an unoccupied N-glycosylation site (site N_{64} NA2) is marked in brown, while the sequence of a peptide containing site N_{38}, that was only detected in recombinant receptor, is indicated in red. Amino acids in yellow show the sequence variations between NA1 and NA2.*

Neither peptides nor glycopeptides corresponding to the glycosylation site N_{38} were observed in our LC-MS/MS data of the healthy donors. Of note, we were able to detect complex glycans occupying site N_{38} on recombinant FcγRIIIb (**Figure S3 and S4**). Yagi *et al.* previously reported on site N_{38} large, highly elaborated glycan structures in the range of *m/z* 1400 to *m/z* 2000.(37) The identified features on recombinant FcγRIIIb possess on average less antennae which are also less processed.

4.4.3 Glycopeptide identification

10 *N*-glycan compositions at N_{45}, 15 at N_{74}, 30 at N_{162} and 6 at N_{169} were identified. Of these 61 compositions, 36 glycoforms were confirmed by tandem mass spectrometry (**Table S4**). Based on glycopeptide fragmentation data, mass accuracy, isotopologue pattern and biosynthetic pathways, we propose the *N*-glycan structures shown in **Figure 2 and S5**.

Numerous structural isomers could be present for the same *N*-glycan composition. We identified multiple isomeric structures, but were not able to resolve them quantitatively. We confirmed the presence of sialic acid by the diagnostic ion at *m/z* 292.103. Antennary fucosylation was confirmed by presence of a B-ion at *m/z* 512.197 [hexose+*N*-acetylhexosamine+fucose+H]$^+$. In contrast, core fucosylation was indicated by the formation of the ion assigned as [peptide+*N*-acetylhexosamine+fucose+H]$^+$. *N*-glycans containing *N*-acetyllactosamine (LacNAc) repeats, were indicated by signals at *m/z* 731.272 [*N*-acetylhexosamine$_2$+hexose$_2$+H]$^+$.

Two novel (N_{74}, N_{169}) and three already described (N_{45}, N_{64}, N_{162}) *N*-glycosylation sites of neutrophil-derived FcγRIIIb were identified. Per site, the nature and number of the glycans differ, and, among other things reflect the extent of biosynthetic processing. The glycan heterogeneity ranges from oligomannose type glycans to highly processed complex type glycans with LacNAc extensions. Three *N*-glycosylation sites, N_{45}, N_{162} and N_{169}, were found to be fully occupied. Glycosylated and non-glycosylated forms of the peptide containing site N_{74} indicated partial occupancy. This peptide was estimated to be glycosylated at 80%, 64% and 58% for donors 1, 2 and 3, respectively. Site N_{64} was known to be unoccupied(36) and indeed corresponding peptides were exclusively non-glycosylated. Molecular dynamics simulations of the highly homologous FcγRIIIa (V158 allotype) have shown intramolecular interactions between the peptide backbone residues 60 to 70 and glycans at N_{45}, which may explain a preference for an unoccupied site N_{64}.(30) Moreover, this intramolecular interaction may inhibit enzymatic *N*-glycan processing in the Golgi, explaining the restricted processing at site N_{45}. The occupancy of site N_{64} appears to be the most prominent difference between neutrophil-bound and soluble FcγRIIIb (**Table S8**); the former unoccupied, the latter displaying highly branched glycans on site N_{64}.(37) Different glycosylation profiles of resting neutrophil-bound FcγRIIIb and soluble FcγRIIIb, released by activated neutrophils,(23) may warrant further study.

MS spectra obtained for sites N_{162} and N_{45} with annotation of the major glycoforms are given in **Figure 3** and **Figure S6**. For site N_{162}, complex di- and triantennary glycans were found accompanied by a small percentage of oligomannose glycans. Site N_{45} mainly showed oligomannosidic glycans with a significant fraction of hybrid and complex structures. N_{74} predominantly elaborated as di- to tetraantennary complex glycans with a small amount of oligomannose type glycans. N_{169} was found to exclusively carry di- and triantennary complex glycans.

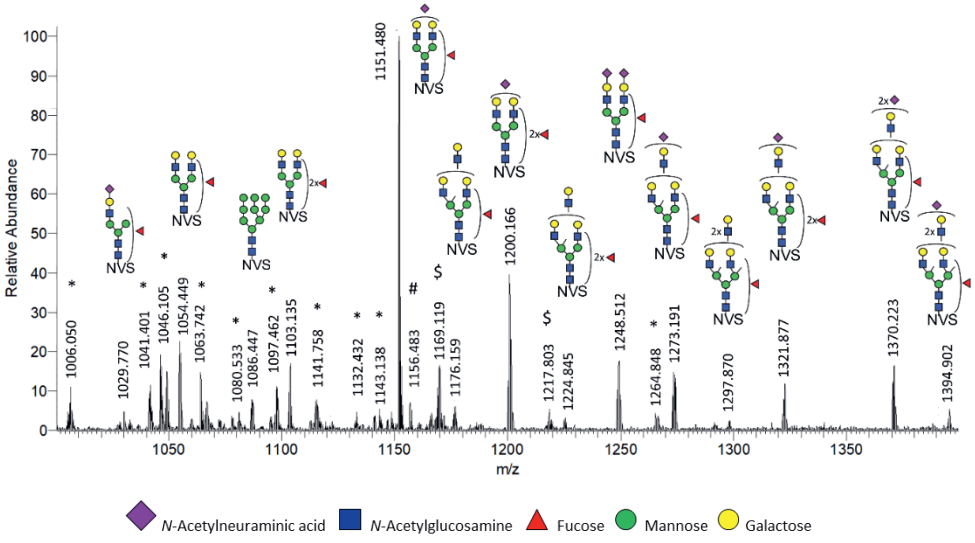

Figure 3. *Sum spectra showing the major glycoforms of the N_{162} site. MS sum spectrum (retention time 10.2 to 14.4 min; 94 spectra) showing the major glycoforms of the N_{162} site. Interestingly, ammonia adducts were exclusively observed for glycopeptides carrying an oligomannose glycan, while iron adducts were detected for both oligomannose and complex structures. For more details on MS/MS spectrum see* ***Figure S9****. *: N_{162} glycopeptides with a miscleaved peptide backbone; #: unidentified glycopeptide (z=2); $: iron adducts $[M+Fe^{III}]^{3+}$. NVS: CRGLVGSK**N**$_{162}$VSSE peptide backbone.*

4.4.4 Site-specific quantification of FcγIIIb *N*-glycans from human neutrophils

The 61 identified glycopeptides were targeted for relative quantification in a site-specific manner (**Figure 4**). FcγRIIIb glycosylation of the three healthy donors displayed very similar glycosylation patterns (**Figure S7**). Derived glycosylation traits — complexity, number of fucoses per glycan and number of sialic acids per glycan — were calculated to facilitate the comparison of the different sites (**Figure S8)** and with other studies (**Table S9**).

As shown in **Figure 4a** and **Table S8,** site N_{45} was decorated with 86% oligomannose type glycans (M6, M7, M8, M9). Remainders were 7% hybrid (M4A1G1S1, M5A1G1S1, FM4A1G1S1) and 8% complex (A1G1S1, FA1G1S1) type glycans, with and without core fucose. In contrast to soluble FcγRIIIb, containing only oligomannose *N*-glycans,(36) the neutrophil-bound N_{45} contains a significant amount of sialylated hybrid and monoantennary complex *N*-glycans.

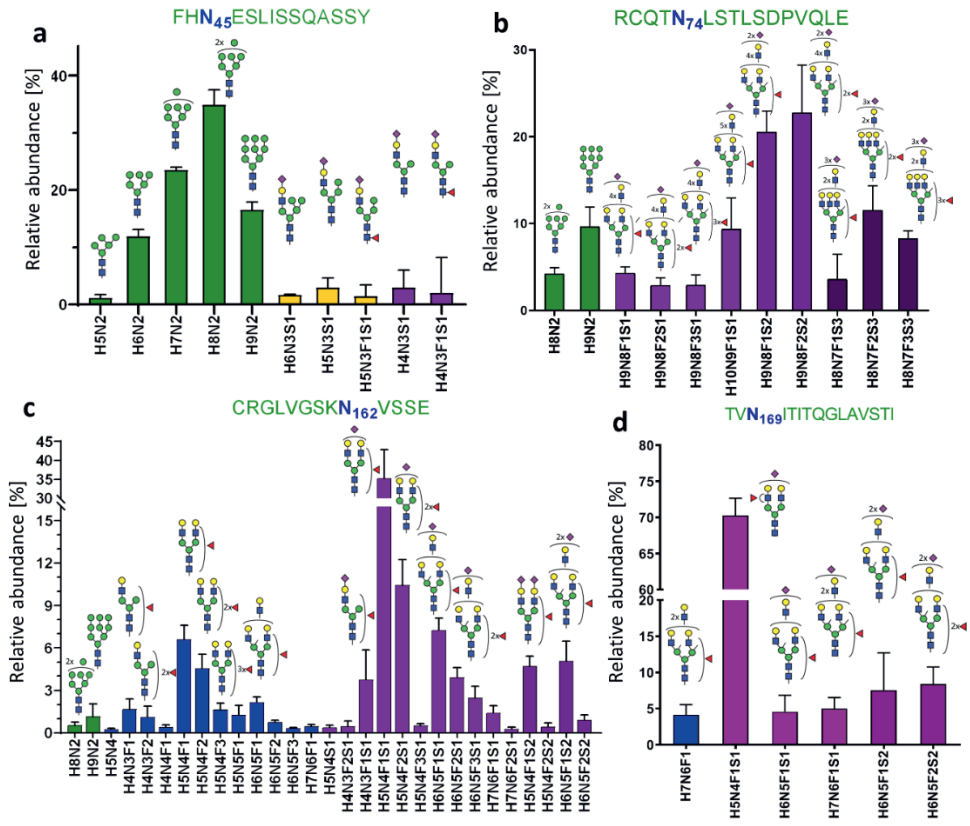

Figure 4. *Site-specific, relative quantification of FcγRIIIb glycoforms. (a) 10 different glycan compositions occupy the glycosylation site N_{45}, (a) 11 compositions on N_{74}, (c) 29 compositions on N_{162} and (d) 6 compositions on N_{169}. Mean and SD of three donors are shown. Bar colours indicate glycan classes: Green, oligomannose type; orange, hybrid type; blue, neutral complex; purple, sialylated complex, with one (light), two (medium) or three (dark) sialic acids per glycan.*

Site N_{162} contained 98% of sialylated, complex, mono- up to triantennary glycans, with some evidence of LacNAc repeats, and 2% of oligomannose glycans (**Figure 4c)**. The derived traits revealed a high level of galactosylation and fucosylation, which indicate a high expression of both galactosyltransferases and fucosyltransferases (**Figure S8**). On average, 1.3 fucoses per glycan were displayed on N_{162} glycans. Diagnostic ions indicated core fucosylation and antennary fucosylation. Some monofucosylated compositions (H5N4F1S1, H5N4F1) also showed evidence of both core and antennary fucosylated isomers. In comparison to the other glycosylation sites, N_{162} possesses the lowest amount of sialic acids per glycan (0.9), which implies poorer accessibility for sialyltransferases.

On site N_{74}, sialylated, fucosylated, complex *N*-glycans with multiple LacNAc extensions represent the largest group (86%) of structures (**Figure 4b**). Fragmentation of these glycans resulted in the formation of the oxonium ion of *m/z* 657.237, assigned as [*N*-

acetylglucosamine+galactose+*N*-acetylneuraminic acid]$^+$ (**Table S4**). No evidence for the presence of oligosialylated antennae was seen in the fragments indicating that the tri-sialylated structures are at least triantennary. Even though N_{74} is not directly involved in antibody binding,(49) there are some speculations regarding LacNAc repetition in cell activation regulation through the modulation of receptor clustering.(50) This site is characterized by the highest numbers of sialic acids (2.1) and fucoses (1.5) per glycan, which implies a high accessibility for sialyltransferases and fucosyltransferases.

Site N_{169} is mainly occupied by a diantennary and monosialylated (H5N4F1S1) structure (**Figure 4d**). Interestingly, core fucosylation at N_{169} was reported for soluble FcγRIIIb, whereas we only observed evidence for antennary fucosylation (**Table S4**). In general, as depicted in **Figure S8**, *N*-glycans modifying N_{169} were fully galactosylated and exhibited a moderate number of sialic acids (1.1) and fucoses (1.1) per glycan.

Overall, we confirmed the presence of antennary fucosylated glycans for three *N*-glycosylation sites, namely N_{74}, N_{162}, and N_{169} (**Table S4**). N_{74} and N_{169} were annotated as predominantly occupied by antennary fucosylated structures, lacking evidence for core fucosylation. In contrast, glycans on N_{162} presented a mixture of both core and antennary fucosylated isomers. In addition to complex type species, oligomannose structures (M8, M9) complement the repertoire of N_{74} (14%) and N_{162} (2%). For N_{74}, oligomannose structures are being reported for the first time. Interestingly, LacNAc repeats were also detected for some N_{162} glycans (**Table S4**). Generally, the presence of oligomannose type glycoforms is not expected among highly processed glycopeptides. However, it is consistent with a recent glycomics study of FcγRIIIa(24) and with a recent study mapping subcellular glycans during cell maturation in healthy human neutrophils,(51) where different stages of *N*-glycan processing within one site may reflect the developmental stage of granulopoiesis.(51) *N*-glycan processing is initially influenced by the protein expression and precursor availability. Differential processing of the sites, however, is influenced by transferase accessibility which seems to correlate with solvent accessibility. The more exposed an *N*-glycosylated asparagine residue is, the more processed its glycans generally are.(52) Additionally, the large biosynthetic gap between the oligomannose type glycans and the large, (at least partially) tetraantennary glycans may indicate different subcellular fractions. Considering the overall glycosylation pattern of FcγRIIIb in neutrophils, we estimated that nearly all glycans of FcγRIIIb were fully galactosylated, indicating a high activity of galactosyltransferases. Consequently, the partially sialylated and core fucosylated glycans suggest a moderate activity of sialyltransferases and α1,6-fucosyltransferases. Lastly, the high average number of fucose per glycan and MS/MS data for antennary fucosylation were evidence for a high activity of α1,2, α1,3 or α1,4 fucosyltransferases in the neutrophils (**Figure S8b, Table S9**).

4.4.5 Comparison of site-specific *N*-glycosylation of FcγRIIIb

Sites N_{74} and N_{169} of neutrophil-bound FcγRIIIb are profiled for the first time. Otherwise, glycosylation profiles were, both qualitatively and quantitatively, highly consistent between the study of Washburn *et al.* and ours (**Table S8 and Table S9)**.(36) A minor difference is the observation of oligomannose *N*-glycans at site N_{162} in our study.

Recently, the site-specific glycosylation of human NK cell FcγRIIIa was published.(24) Major glycosylation differences in sites $N_{45,}$ N_{74} and N_{169} clearly distinguish the two FcγRIII isoforms (**Table S8 and S9**). FcγRIIIb showed less processing than FcγRIIIa on N_{45}, having mainly oligomannose glycans, while FcγRIIIa expressed mainly hybrid type glycans. The most pronounced differences were observed in the levels of antennary fucosylation. FcγRIIIb had on average more than one fucose per glycan, up to 1.5 on N_{74}. Moreover, only antennary fucosylation was observed for monofucosylated glycans at site N_{169}. In stark contrast, glycoforms of FcγRIIIa are reported to be almost exclusively core fucosylated, except small amounts of antennary fucosylation on sites N_{74} and N_{162}. This hints at a higher activity of α1,2, α1,3 or α1,4 fucosyltransferases in the neutrophils versus NK cells. *N*-glycans at N_{162} showed the highest similarity between the two receptor isotypes. This observation suggests that the glycosylation profiles of this functionally relevant site are conserved among FcγRIII isoforms and cells. However, sialylation of N_{162} appeared lower in neutrophil FcγRIIIb than in NK cell FcγRIIIa with 0.9 and 1.3 sialic acids per glycan at N_{162}, respectively.

Notably, glycosylation differences influence FcγRIII properties and function.(34) Thus, it is important to use an expressing system that assembles an endogenous-like glycosylation profile for *in-vitro* studies. Among all four mammalian systems producing differently processed *N*-glycans (HEK293, CHO, BHK, NS0),(26-28) CHO cells constitute a good expression vehicle, where the highly-branched N_{74} glycans in FcγRIII were carrying LacNAc repetitions. However, to produce antennary fucosylation, prevalent in FcγRIIIb, the HEK293 system constitutes a better vehicle. Additionally, glycoengineering allows to create specific FcγRIIIb structures for functional studies.(53, 54) The present data indicate that neutrophil-derived FcγRIIIb *N*-glycosylation is rather consistent between healthy individuals, but significantly differs from soluble FcγRIIIb, recombinant or serum-derived, and NK cell-derived FcγRIIIa profiles.

4.5 CONCLUSION

In this study, we describe a straightforward and comprehensive site-specific profiling of FcγRIIIb *N*-glycosylation with a resolution of a single donor. However, by design the approach may be applicable to many different leukocytes.

The observed differences between the plasma-derived and the neutrophil-derived FcγRIIIb demonstrate a significant biological diversity. It would be of great interest to compare FcγRIIIb glycosylation profiles of subcellular fractions or FcγRIIIb from resting neutrophils to soluble receptors in the same donor. The source and impact of the simultaneous similarity,

site N_{162}, and dissimilarity, other sites, between FcγRIIIb and FcγRIIIa glycosylation warrants further study as well.

Additional isomer differentiation would also be desirable, but would likely need a separation method with a higher degree of isomers separation.

We believe that a throughput-optimized adaptation of the presented approach could be used in defining glycan signatures of FcγRIII for different pathophysiological conditions in various cell types or even subcellular compartments. This would reveal a yet hidden layer of regulation of antibody-mediated (auto-)immune responses. However, sensitivity should be further improved for such aims. A better understanding of glycosylation as an additional layer of regulation of FcγR activity is likely to improve the performance of antibody-based therapeutic interventions and provide clinical markers for personalized medicine in the long run.

4.6 ACKNOWLEDGMENTS

We thank Gillian Dekkers for expressing the recombinant receptors used in the initial development of the method. This research was supported by the European Union (Glycosylation Signatures for Precision Medicine project, GlySign, Grant No.722095), and the Netherlands Organization for Scientific Research (NWO) via Vernieuwingsimpuls Veni (Project No.722.016.008) and Medium Investment (to P.A.V.; 91116004; partly financed by ZonMw) grants.

4.7 SUPPLEMENTARY MATERIAL

A complete overview of the supplementary material is available online at https://pubs.acs.org/doi/10.1021/acs.analchem.0c02342.

Table S1. *Information on healthy donors and separated neutrophils cells used for FcγRIIIb isolation.*

	Donor 1	Donor 2	Donor 3
Sex	female	male	female
Cell type	neutrophils	neutrophils	neutrophils
Cell count [cell/mL]	$50x10^6$	$50x10^6$	$50x10^6$
Total protein con. [mg/mL]	1.61	1.72	1.51
Amount of cells for isolation [cell/mL]	$16x10^6$	$15x10^6$	$17x10^6$
Volume of lysate for isolation [µL]	310	291	331
Amount of total protein for isolation [µg]	500	500	500

Table S3. *The search parameters used for initial analysis using Byonic (Protein Metrics, Cupertino, CA v3.2-38).*

Search parameter	Value
Protein database	UniProt human protein database
Glycan database	User defined, see Table S2
Precursor mass tolerance	5 ppm
Fragmentation type	QTOF/HCD
Parent tolerance	0.005 *m/z*
Fragment mass tolerance	20 ppm
Recalibration (lock mass)	none
Maximum precursor mass	10,000
Precursor and mass charge assignments	compute from MS1
Max # of precursor per scan	2
Smoothing width	0.01 *m/z*

Table S5. *Byonic output of critical parameters reflecting the quality of the peptide-spectrum matches (PSMs) of identified FcγRIIIb for each donor. The list of parameters includes: protein p-value (the likelihood of the PSMs to be the identified protein). # unique peptides (total number of PSMs). coverage % (percent of the protein sequence covered by PSMs).*

Donor	Protein Identificeer	Protein p-value (Log base 10)	# unique peptides	Ranking place	Coverage
1	Low affinity immunoglobulin gamma Fc region receptor III-B UNIPROT: O75015 (FCG3B_HUMAN)	362.01	131	1	77.8 %
2		268.28	127	1	80.3 %
3		250.22	114	1	71.2 %

Table S6. *Characterization of predominant human FcγRIIIb (UniProtKB - O75015) site-specific peptides and glycopeptides generated from Endoproteinase Glu-C and chymotrypsin cleavage. C, carboxymethyl cysteine*

Site	Peptide sequence	Glycosylation	*m/z* peptide [M+H]	*m/z* peptide [M+GlcNAc]	RT [min]
Asn 38	missing peptide	NA	NA	NA	NA
Asn 45	FHN(45)ES(47)LISSQASSY	+	1569.708	1772.787	17 - 23
Asn 64	FIDAATVN(64)DSGEY	-	1401.617	1604.696	19
Asn 74	RCQTN(74)LSTLSDPVQLE	+	1860.901	2063.980	20-28
	RCQTN(74)LSTLSDPVQLE	-	1860.901	-	25
Asn 162	CRGLVGSKN(162)VSSE	+	1392.679	1595.758	10 - 14
Asn 169	TVN(169)ITITQGLAV	+	1229.706	1432.779	28 - 32

Table S7. *Allelic peptide and glycopeptide sequences containing N45 and N64/D64 used for polymorphic variant assessment. *Uniprot identifiers.*

FcγRIII variant	N_{45} peptide	N_{64} peptide
NA1 *O75015 (FCG3B*01)	FHN$_{45}$EN(47)LISSQASSY	FIDAATVD$_{64}$DSGEY
NA2 *O75015 (FCG3B*02)	FH**N**$_{45}$ES(47)LISSQASSY	FIDAATV**N**$_{64}$DSGEY
FcγRIIIa *P08637	FH**N**$_{45}$ES(47)LISSQASSY	FIDAATVD$_{64}$DSGEY

DONOR	RATIO ALLOTYPIC		ALLOTYPE
	NES/(NES+NEN)	NDS/(DDS+NDS)	
Donor 1	0.2	0.26	NA1/NA2
Donor 2	0.99	0.98	NA2/NA2
Donor 3	0.99	0.98	NA2/NA2

Table S8. *The glycosylation profiles of endogenous neutrophil-derived FcγRIIIb, soluble FcγRIIIb and NK-derived FcγRIIIa. The different glycoforms are displayed as defined derived traits (high mannose, complex, hybrid). *the corresponding glycopeptides were not detected in this study **potential glycosylation site was not occupied by oligosaccharides, only corresponding peptide observed.*

Sites	FcγRIIIb – our study (human neutrophils)	sFcγRIIIb(37) (human serum)	FcγRIIIb(36) (human neutrophils)	FcγRIIIa(24) (human natural killer cells)
N_{38}	-*	Complex (LacNAc repeats) > 99%	- *	Complex (LacNAc repeats) > 99%
N_{45}	Complex (monoantennary) 8% Hybrid 7% High mannose 86%	High mannose >99%	Complex (monoantennary) 16% Hybrid < 30% High mannose 54%	Complex (di-, tri-, tetra antennary) 22% Hybrid 71% High mannose 2%
N_{64}	-** (not glycosylated)	Complex (LacNAc repeats) > 99%	- ** (not glycosylated)	-
N_{74}	Complex (LacNAc repeats) 86% High mannose 14%	Complex (LacNAc repeats) > 99 %	- *	Complex (LacNAc repeats) > 99%
N_{162}	Complex (mono-, di- , tri antennary) 98% High mannose 2%	Complex (di-, tri-, tetraantennary) > 99%	Complex (di-, tri antennary) > 99%	Complex (di-, tri-antennary) 66% Hybrid 22% High mannose 12%
N_{169}	Complex (di-, tri-, tetrantennary) > 99%	Complex (di-, tri-, tetrantennary) > 99%	- *	Complex (di-, tri-, tetrantennary) > 99%

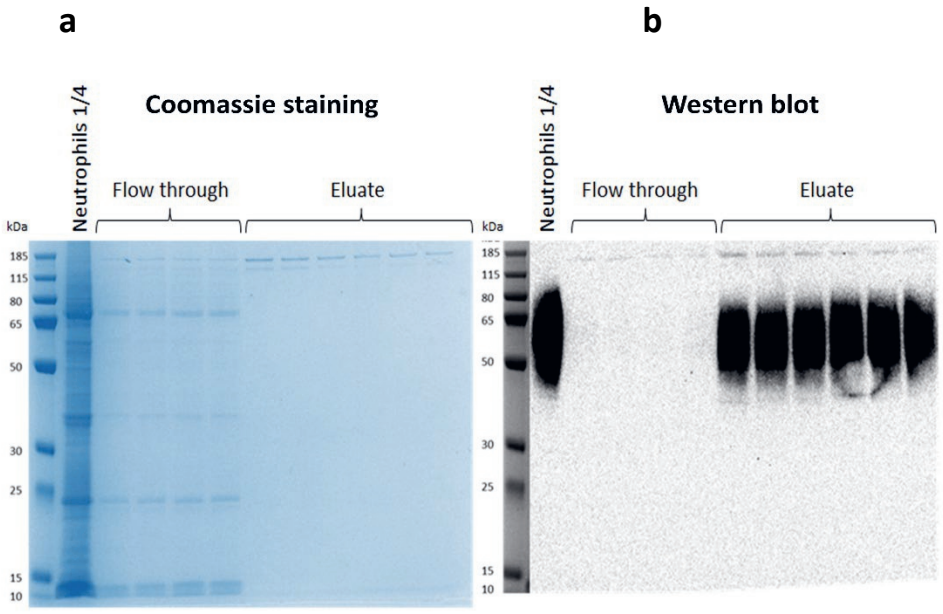

Figure S1. *The whole non-reducing SDS-PAGE and western blot of human neutrophil lysate before and after FcγRIII immunoprecipitation. Protein contaminations and FcγRIIIb were detected with (**a**) coomassie staining and (**b**) western blot, respectively. The neutrophil lanes represent ~25 µg of total protein content from the neutrophil cell lysate from donor 2. In this experiment, the immunoprecipitation was done from 100 µg and the eluate was split between the two gels (50 µg per gel). The flow-through lanes show the unbound diluted fraction of the immunoprecipitation while the eluate lanes present the purified FcγRIIIb protein. As expected, FcγRIIIb exhibits an elongated band from 50 to 80 kDa, visible after western blotting. Despite high dilution, the flow-through mirrors the major bands from the total cell lysate. In contrast, the eluate exhibits none of those bands and thus any interfering proteins of 50-80 kDa above the limit of detection (LOD; 25 ng protein). Two bands around 150 kDa appear in the flow-through and eluate. They are likely derived from the capturing antibody, as an in-solution proteolytic cleavage of the eluate revealed immunoglobulin G glycopeptide masses (data not shown). Whatever the identity of the contamination, it is the main reason to prefer an in-gel proteolytic cleavage.*

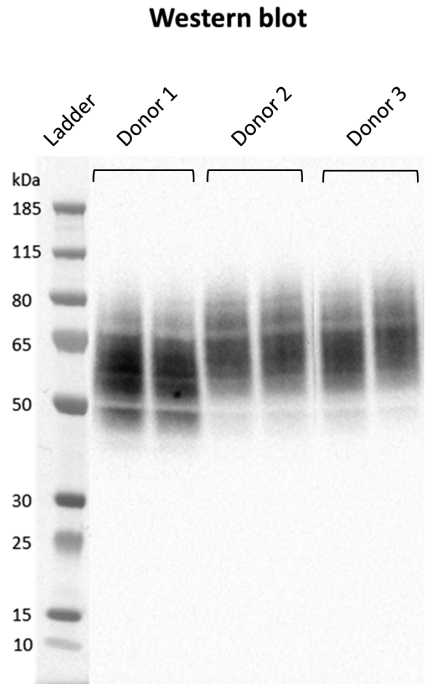

Figure S2. *The immunoblot shows FcγRIIIb immunoprecipitated from the lysate of neutrophils. Lanes contain material from donor 1 (NA1/NA2), donor 2 (NA2/NA2) and donor 3 (NA2/NA2) in duplicate. Size markers are indicated on the left. FcγRIIIb showed a smear from 50 to 80 kDa indicating the heterogeneity of the N-glycosylation pattern of the receptor. Differential electrophoretic mobility of the receptor from NA1/NA2-heterozygous and NA2-homozygous is likely mainly due to NA polymorphism and distinct number of N-glycosylation sites.(23) Larger proteoforms attributed to NA2, may not be visible in the first donor, because the protein expression is skewed towards NA1.*

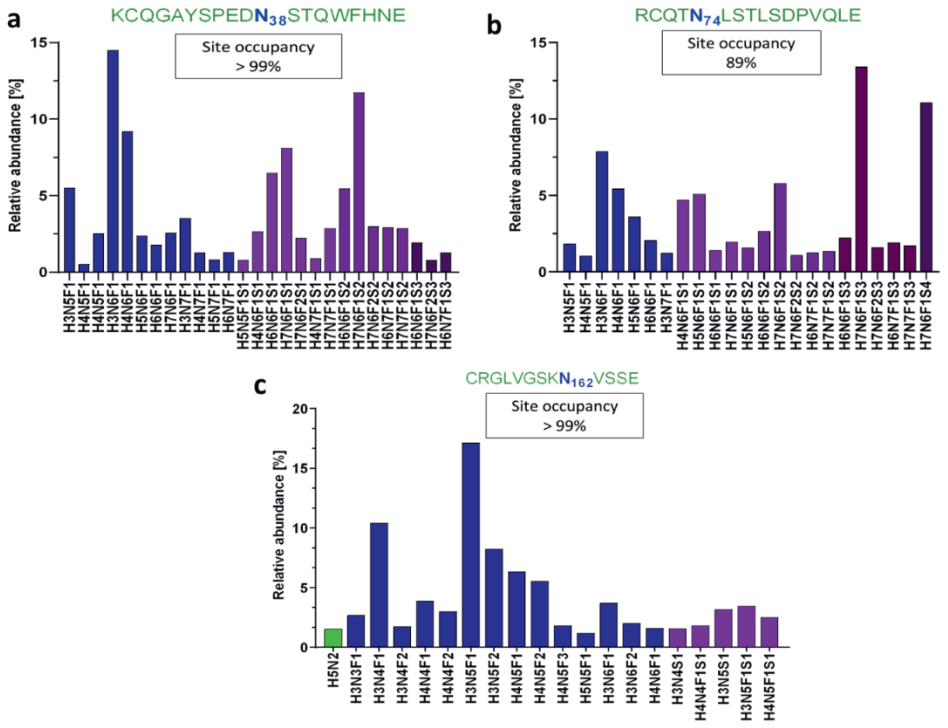

Figure S3. *Bar graphs showing the relative abundances of identified glycopeptides for recombinant NA1 allotype of FcγRIIIb(55). Site-specific analysis revealed (a) 27 different glycan compositions occupying the glycosylation site N_{38}, (b) 54 compositions on site N_{74} and (c) 65 compositions on site N_{162}. For sites N_{74} and N_{162} only compositions above a 1% cut-off of relative abundance were visualized, amounting to 23 and 20 glycans respectively. Full glycosylation site occupancy was observed for N_{38} and N_{162}, while site N_{74} was partially occupied. 11% relative signal intensity of the non-glycosylated peptide were detected. Sulphated and multifucosylated N-glycan compositions were detected below 1% relative intensity for N_{74}, as were sulphated and disialylated N-glycans for N_{162}. Bar colours indicate glycan classes: Green, oligomannose type; blue, neutral complex; purple, sialylated complex, with one (light), two (medium) or three (dark) sialic acids per glycan.*

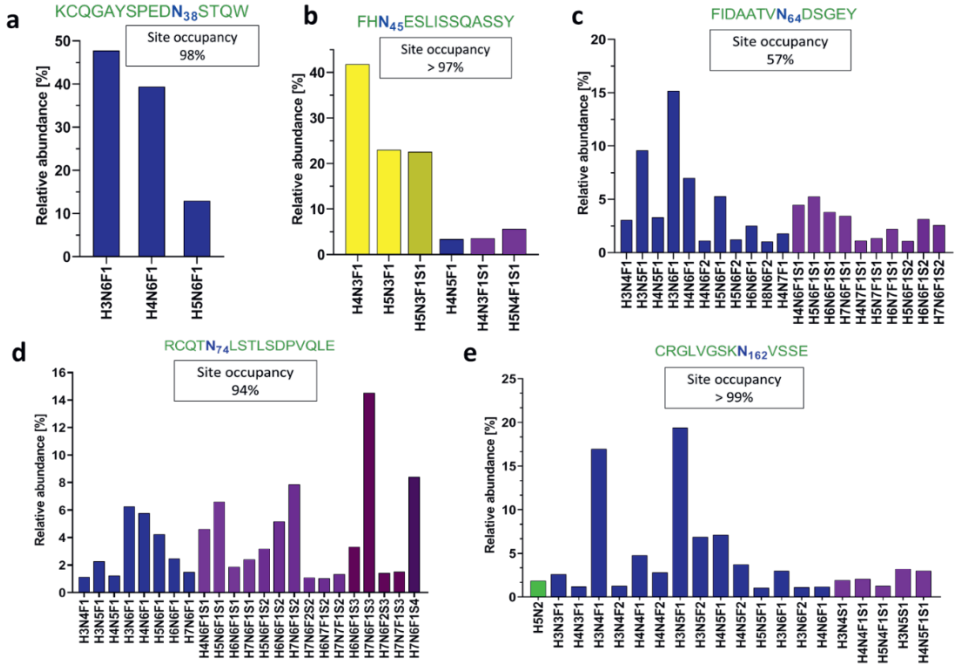

Figure S4. *Bar graphs showing the relative abundances of identified glycopeptides for the recombinant NA2 allotype of FcγRIIIb(55). Site-specific analysis revealed (a) 3 different glycan compositions occupying the glycosylation site N_{38}, (b) 6 compositions on site N_{45}, (c) 35 compositions on site N_{64}, (d) 49 compositions on site N_{74} and (e) 69 compositions on site N_{162}. For sites N_{64}, N_{74} and N_{162} only compositions above a 1% cut-off of relative abundance were visualized, amounting to 21, 23 and 20 glycans respectively. Full glycosylation site occupancy was observed for N_{45} and N_{162}, while sites N_{38}, N_{64} and N_{74} were partially occupied. 2%, 46% and 7% relative signal intensity of the non-glycosylated peptide for sites N_{38}, N_{64} and N_{74} were detected respectively. Multifucosylated N-glycan compositions for N_{64}, sulfated N-glycans for N_{74} and sulphated and disialylated N-glycans for N_{162} were detected below 1% relative intensity. Bar colours indicate glycan classes: Yellow, hybrid, sialylated hybrid (medium); Green, oligomannose type; blue, neutral complex; purple, sialylated complex, with one (light), two (medium) or three (dark) sialic acids per glycan.*

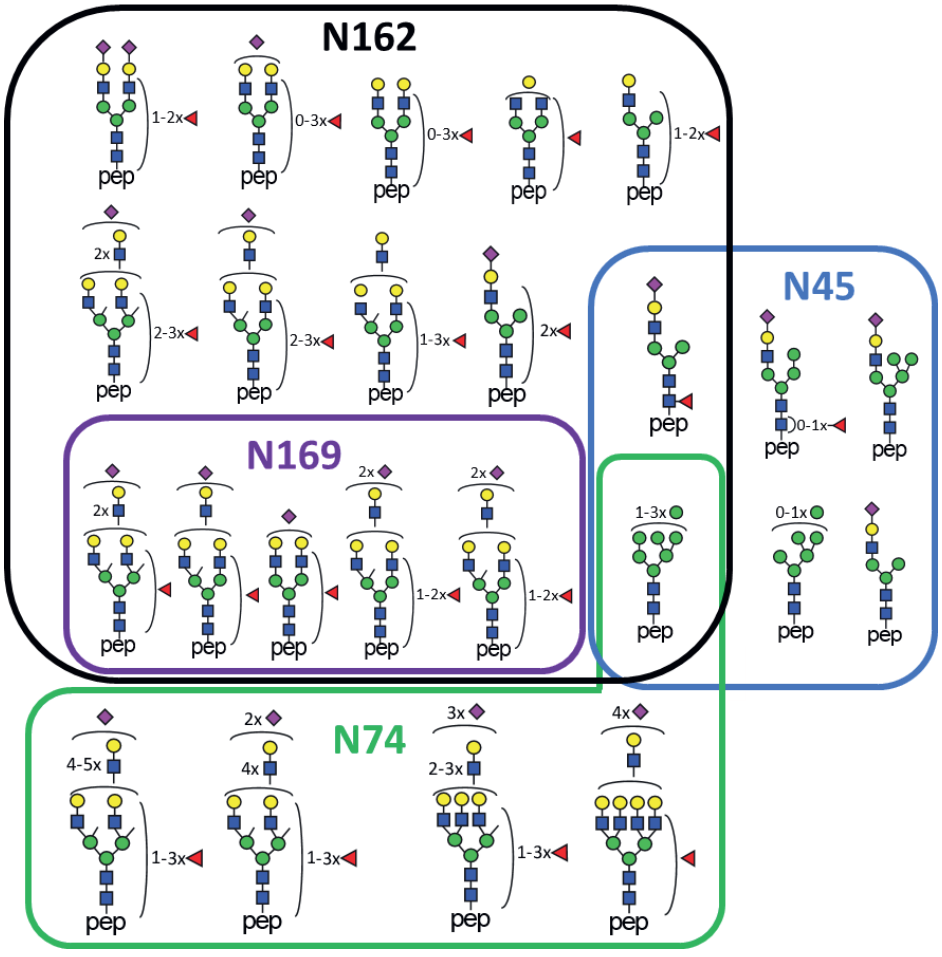

Figure S5. *Putative structures of N-glycans identified on the four occupied N-glycosylation sites, namely 10 at N_{45}, 15 at N_{74}, 30 at N_{162} and 6 at N_{169}. Isomeric structures co-occur and are discussed in the text. The scheme underlines the diversity, overlap and uniqueness of glycans compositions.*

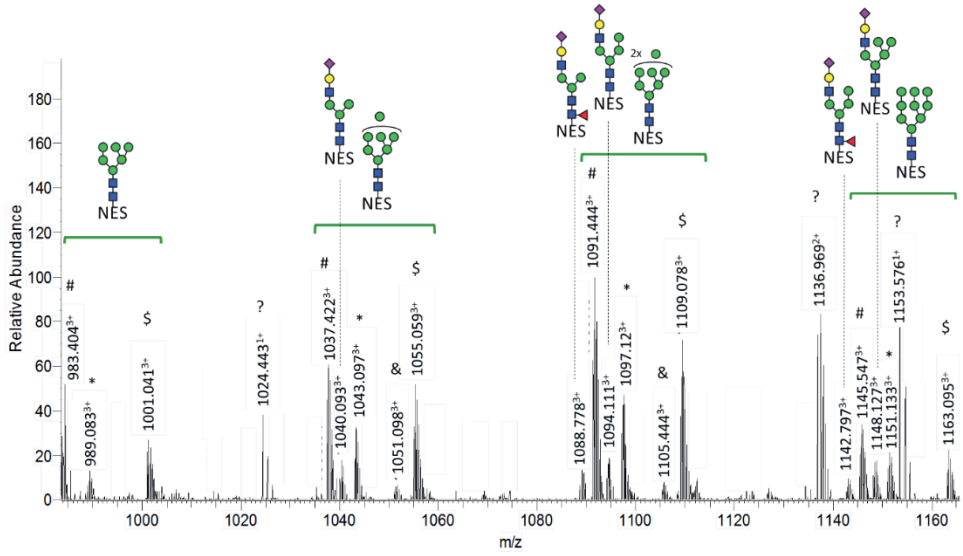

***Figure S6**. Sum spectra showing the different ions observed for the N_{45} glycoforms of FcγRIIIb. The mass spectrum was generated for donor 2 within the following retention time range: 17.4-19.4 min. NES: FH**N_{45}**ESLISSQASSY peptide backbone. The MS spectra revealed satellite peaks for some triply-charged protonated species with a difference of 55.934 Da and 18.033 Da. These were identified by accurate mass (< ± 5 ppm) as iron ($[M+Fe^{III}]^{3+}$) and ammonia ($[M+2H+NH_4]^{3+}$) adducts, respectively. They also presented the same retention time as the respective protonated glycopeptide. Additionally, the presence of the ammonia adducts was confirmed by MS/MS spectra, as the comparison of the b-and y-ion series provided evidence for the same peptide backbone without additional modification. #: the triply protonated N_{45} glycopeptides $[M+3H]^{3+}$. *: the triply charged ions of protonated N_{45} glycopeptides with ammonia adducts $[M+2H+NH_4]^{3+}$. $: N_{45} glycopeptides charged by iron ions $[M+Fe^{III}]^{3+}$. &: misscleaved glycopeptide. ?: unidentified glycopeptide.*

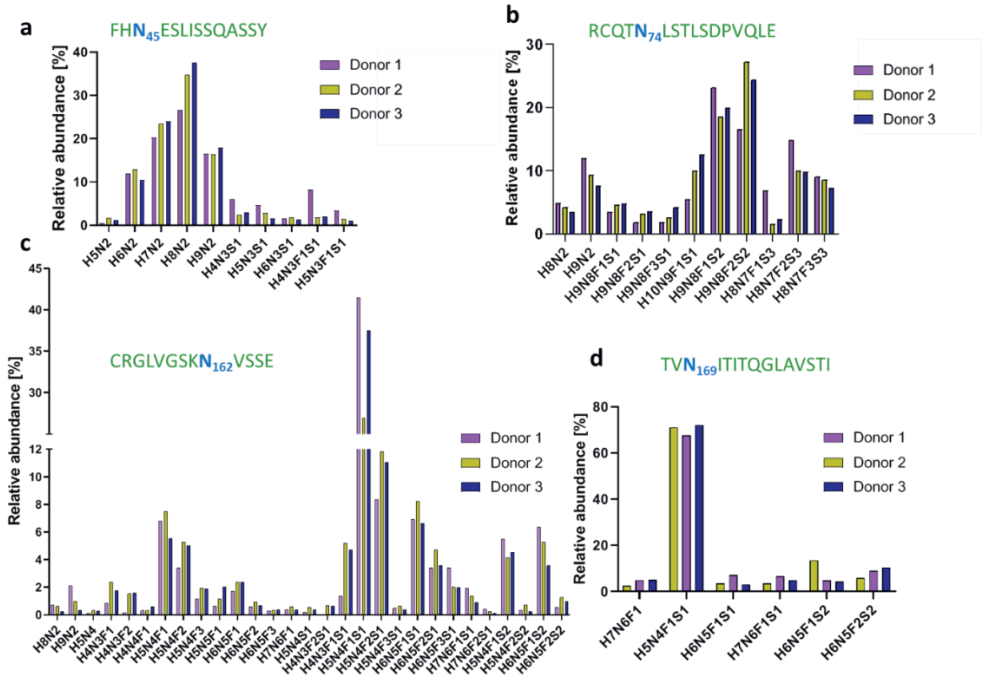

Figure S7. *Site-specific relative quantification of FcγRIIIb glycoforms. Bar graphs show the relative abundance of identified glycopeptides for individual donors, donor 1 (NA1/NA2), donor 2 (NA2/NA2) and donor 3 (NA2/NA2). (a) 10 different glycan compositions occupy glycosylation site N_{45}, (b) 11 site N_{74}, (c) 30 site N_{162} and (d) 6 site N_{169}.*

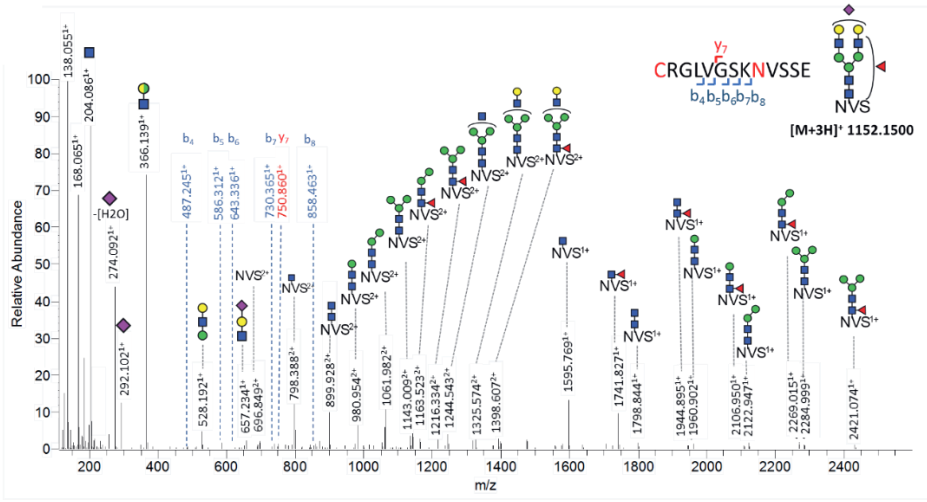

Figure S9. *Stepping-energy HCD MS/MS sum spectrum of the precursor ion 1152.150^{3+} [second isotopologue] of the most abundant N_{162} glycopeptide (H5N4F1S1). The MS/MS spectrum was generated for three stepping energies (32%, 37%, 42% NCE) at retention time 11.0 min.*

4.8 REFERENCES

1. Nimmerjahn F, Ravetch JV. Fcgamma receptors as regulators of immune responses. Nat Rev Immunol. 2008;8(1):34-47.
2. Kapur R, Einarsdottir HK, Vidarsson G. IgG-effector functions: "the good, the bad and the ugly". Immunol Lett. 2014;160(2):139-44.
3. Ben Mkaddem S, Benhamou M, Monteiro RC. Understanding Fc Receptor Involvement in Inflammatory Diseases: From Mechanisms to New Therapeutic Tools. Front Immunol. 2019;10:811.
4. Bournazos S, Woof JM, Hart SP, Dransfield I. Functional and clinical consequences of Fc receptor polymorphic and copy number variants. Clin Exp Immunol. 2009;157(2):244-54.
5. Hogarth PM, Pietersz GA. Fc receptor-targeted therapies for the treatment of inflammation, cancer and beyond. Nat Rev Drug Discov. 2012;11(4):311-31.
6. Hudis CA. Trastuzumab--mechanism of action and use in clinical practice. N Engl J Med. 2007;357(1):39-51.
7. Schwab I, Nimmerjahn F. Intravenous immunoglobulin therapy: how does IgG modulate the immune system? Nat Rev Immunol. 2013;13(3):176-89.
8. Cobb BA. The history of IgG glycosylation and where we are now. Glycobiology. 2020;30(4):202-13.
9. de Haan N, Falck D, Wuhrer M. Monitoring of immunoglobulin N- and O-glycosylation in health and disease. Glycobiology. 2020;30(4):226-40.
10. Vidarsson G, Dekkers G, Rispens T. IgG subclasses and allotypes: from structure to effector functions. Front Immunol. 2014;5:520.
11. Yamaguchi Y, Barb AW. A synopsis of recent developments defining how N-glycosylation impacts immunoglobulin G structure and function. Glycobiology. 2020;30(4):214-25.
12. de Taeye SW, Bentlage A, Mebius MM, Meesters JI, Lissenberg S, Falck D, et al. FcγR binding and ADCC activity of human IgG allotypes Front Immunol. 2020.
13. Rosales C. Fcgamma Receptor Heterogeneity in Leukocyte Functional Responses. Front Immunol. 2017;8:280.
14. Hayes JM, Cosgrave EF, Struwe WB, Wormald M, Davey GP, Jefferis R, et al. Glycosylation and Fc receptors. Curr Top Microbiol Immunol. 2014;382:165-99.
15. Bruhns P, Iannascoli B, England P, Mancardi DA, Fernandez N, Jorieux S, et al. Specificity and affinity of human Fcgamma receptors and their polymorphic variants for human IgG subclasses. Blood. 2009;113(16):3716-25.
16. Roberts JT, Barb AW. A single amino acid distorts the Fc gamma receptor IIIb/CD16b structure upon binding immunoglobulin G1 and reduces affinity relative to CD16a. J Biol Chem. 2018;293(51):19899-908.
17. Kara S, Amon L, Luhr JJ, Nimmerjahn F, Dudziak D, Lux A. Impact of Plasma Membrane Domains on IgG Fc Receptor Function. Front Immunol. 2020;11:1320.
18. Huizinga TW, Kleijer M, Tetteroo PA, Roos D, von dem Borne AE. Biallelic neutrophil Na-antigen system is associated with a polymorphism on the phospho-inositol-linked Fc gamma receptor III (CD16). Blood. 1990;75(1):213-7.
19. Coxon A, Cullere X, Knight S, Sethi S, Wakelin MW, Stavrakis G, et al. Fc gamma RIII mediates neutrophil recruitment to immune complexes. a mechanism for neutrophil accumulation in immune-mediated inflammation. Immunity. 2001;14(6):693-704.
20. Chen K, Nishi H, Travers R, Tsuboi N, Martinod K, Wagner DD, et al. Endocytosis of soluble immune complexes leads to their clearance by FcgammaRIIIB but induces neutrophil extracellular traps via FcgammaRIIA in vivo. Blood. 2012;120(22):4421-31.
21. Wang Y, Jonsson F. Expression, Role, and Regulation of Neutrophil Fcgamma Receptors. Front Immunol. 2019;10:1958.
22. Salmon JE, Edberg JC, Kimberly RP. Fc gamma receptor III on human neutrophils. Allelic variants have functionally distinct capacities. J Clin Invest. 1990;85(4):1287-95.
23. Huizinga TW, de Haas M, Kleijer M, Nuijens JH, Roos D, von dem Borne AE. Soluble Fc gamma receptor III in human plasma originates from release by neutrophils. J Clin Invest. 1990;86(2):416-23.
24. Patel KR, Nott JD, Barb AW. Primary human natural killer cells retain proinflammatory IgG1 at the cell surface and express CD16a glycoforms with donor-dependent variability. Mol Cell Proteomics. 2019.
25. Roberts JT, Patel KR, Barb AW. Site-specific N-glycan Analysis of Antibody-binding Fc gamma Receptors from Primary Human Monocytes. Molecular & Cellular Proteomics. 2020;19(2):362-74.
26. Zeck A, Pohlentz G, Schlothauer T, Peter-Katalinic J, Regula JT. Cell type-specific and site directed N-glycosylation pattern of FcgammaRIIIa. J Proteome Res. 2011;10(7):3031-9.
27. Kawasaki N, Okumoto T, Yamaguchi Y, Takahashi N, Fridman W, Sautès-Fridman C, et al. Site-Specific Classification of N-Linked Oligosaccharides of the Extracellular Regions of Fcγ Receptor IIIb Expressed in Baby Hamster Kidney Cells. Journal of Glycomics & Lipidomics. 2014;4.

28. Cosgrave EF, Struwe WB, Hayes JM, Harvey DJ, Wormald MR, Rudd PM. N-linked glycan structures of the human Fcgamma receptors produced in NS0 cells. J Proteome Res. 2013;12(8):3721-37.
29. Ferrara C, Grau S, Jager C, Sondermann P, Brunker P, Waldhauer I, et al. Unique carbohydrate-carbohydrate interactions are required for high affinity binding between FcgammaRIII and antibodies lacking core fucose. Proc Natl Acad Sci U S A. 2011;108(31):12669-74.
30. Subedi GP, Falconer DJ, Barb AW. Carbohydrate-Polypeptide Contacts in the Antibody Receptor CD16A Identified through Solution NMR Spectroscopy. Biochemistry. 2017;56(25):3174-7.
31. Shibata-Koyama M, Iida S, Okazaki A, Mori K, Kitajima-Miyama K, Saitou S, et al. The N-linked oligosaccharide at Fc gamma RIIIa Asn-45: an inhibitory element for high Fc gamma RIIIa binding affinity to IgG glycoforms lacking core fucosylation. Glycobiology. 2009;19(2):126-34.
32. Dekkers G, Bentlage AEH, Plomp R, Visser R, Koeleman CAM, Beentjes A, et al. Conserved FcgammaR- glycan discriminates between fucosylated and afucosylated IgG in humans and mice. Mol Immunol. 2018;94:54-60.
33. Hayes JM, Frostell A, Karlsson R, Muller S, Martin SM, Pauers M, et al. Identification of Fc Gamma Receptor Glycoforms That Produce Differential Binding Kinetics for Rituximab. Mol Cell Proteomics. 2017;16(10):1770-88.
34. Subedi GP, Barb AW. CD16a with oligomannose-type N-glycans is the only "low-affinity" Fc gamma receptor that binds the IgG crystallizable fragment with high affinity in vitro. J Biol Chem. 2018;293(43):16842-50.
35. Patel KR, Roberts JT, Subedi GP, Barb AW. Restricted processing of CD16a/Fc gamma receptor IIIa N-glycans from primary human NK cells impacts structure and function. J Biol Chem. 2018;293(10):3477-89.
36. Washburn N, Meccariello R, Duffner J, Getchell K, Holte K, Prod'homme T, et al. Characterization of Endogenous Human FcgammaRIII by Mass Spectrometry Reveals Site, Allele and Sequence Specific Glycosylation. Mol Cell Proteomics. 2019;18(3):534-45.
37. Yagi H, Takakura D, Roumenina LT, Fridman WH, Sautes-Fridman C, Kawasaki N, et al. Site-specific N-glycosylation analysis of soluble Fcgamma receptor IIIb in human serum. Sci Rep. 2018;8(1):2719.
38. Riley NM, Hebert AS, Westphall MS, Coon JJ. Capturing site-specific heterogeneity with large-scale N-glycoproteome analysis. Nat Commun. 2019;10(1):1311.
39. Zhu J, Lin YH, Dingess KA, Mank M, Stahl B, Heck AJR. Quantitative Longitudinal Inventory of the N-Glycoproteome of Human Milk from a Single Donor Reveals the Highly Variable Repertoire and Dynamic Site-Specific Changes. J Proteome Res. 2020;19(5):1941-52.
40. Candiano G, Bruschi M, Musante L, Santucci L, Ghiggeri GM, Carnemolla B, et al. Blue silver: a very sensitive colloidal Coomassie G-250 staining for proteome analysis. Electrophoresis. 2004;25(9):1327-33.
41. Kuijpers TW, Tool AT, van der Schoot CE, Ginsel LA, Onderwater JJ, Roos D, et al. Membrane surface antigen expression on neutrophils: a reappraisal of the use of surface markers for neutrophil activation. Blood. 1991;78(4):1105-11.
42. Shevchenko A, Wilm M, Vorm O, Mann M. Mass spectrometric sequencing of proteins silver-stained polyacrylamide gels. Anal Chem. 1996;68(5):850-8.
43. Shevchenko A, Tomas H, Havlis J, Olsen JV, Mann M. In-gel digestion for mass spectrometric characterization of proteins and proteomes. Nat Protoc. 2006;1(6):2856-60.
44. Gundry RL, White MY, Murray CI, Kane LA, Fu Q, Stanley BA, et al. Preparation of proteins and peptides for mass spectrometry analysis in a bottom-up proteomics workflow. Curr Protoc Mol Biol. 2009;Chapter 10:Unit10 25.
45. Bern M, Kil YJ, Becker C. Byonic: advanced peptide and protein identification software. Curr Protoc Bioinformatics. 2012;Chapter 13:Unit13 20.
46. Jansen BC, Falck D, de Haan N, Hipgrave Ederveen AL, Razdorov G, Lauc G, et al. LaCyTools: A Targeted Liquid Chromatography-Mass Spectrometry Data Processing Package for Relative Quantitation of Glycopeptides. J Proteome Res. 2016;15(7):2198-210.
47. Galon J, Moldovan I, Galinha A, Provost-Marloie MA, Kaudewitz H, Roman-Roman S, et al. Identification of the cleavage site involved in production of plasma soluble Fc gamma receptor type III (CD16). Eur J Immunol. 1998;28(7):2101-7.
48. Breunis WB, van Mirre E, Geissler J, Laddach N, Wolbink G, van der Schoot E, et al. Copy number variation at the FCGR locus includes FCGR3A, FCGR2C and FCGR3B but not FCGR2A and FCGR2B. Hum Mutat. 2009;30(5):E640-50.
49. Sondermann P, Huber R, Oosthuizen V, Jacob U. The 3.2-A crystal structure of the human IgG1 Fc fragment-Fc gammaRIII complex. Nature. 2000;406(6793):267-73.
50. Demetriou M, Granovsky M, Quaggin S, Dennis JW. Negative regulation of T-cell activation and autoimmunity by Mgat5 N-glycosylation. Nature. 2001;409(6821):733-9.
51. Venkatakrishnan V, Dieckmann R, Loke I, Tjondro H, Chatterjee S, Bylund J, et al. Glycan analysis of human neutrophil granules implicates a maturation-dependent glycosylation machinery. J Biol Chem. 2020.

52. Thaysen-Andersen M, Packer NH. Site-specific glycoproteomics confirms that protein structure dictates formation of N-glycan type, core fucosylation and branching. Glycobiology. 2012;22(11):1440-52.
53. Hayes JM, Wormald MR, Rudd PM, Davey GP. Fc gamma receptors: glycobiology and therapeutic prospects. J Inflamm Res. 2016;9:209-19.
54. Buettner MJ, Shah SR, Saeui CT, Ariss R, Yarema KJ. Improving Immunotherapy Through Glycodesign. Front Immunol. 2018;9:2485.
55. Dekkers G, Treffers L, Plomp R, Bentlage AEH, de Boer M, Koeleman CAM, et al. Decoding the Human Immunoglobulin G-Glycan Repertoire Reveals a Spectrum of Fc-Receptor- and Complement-Mediated-Effector Activities. Front Immunol. 2017;8:877.